Improved determination of Europa's long-wavelength topography using stellar occultations

Jacob N. H. Abrahams[1], Francis Nimmo[1], Tracy Becker[2], Randy Gladstone[2], Kurt Retherford[2], Gregor Steinbrügge[3], Erwan Mazarico[4]

[1]Department of Earth and Planetary Science, University of California Santa Cruz, Santa Cruz, CA, USA
[2]Southwest Research Institute: San Antonio, TX, USA
[3]Department of Geophysics, Stanford University, CA, USA
[4]NASA Goddard Space Flight Center, Greenbelt, MD, USA

Key Points:

- Understanding Europa's global shape is important for understanding its ice shell.
- Europa Clipper's primary instruments for measuring topography will be limited in constraining global shape because Clipper orbits Jupiter.
- Stellar Occultations obtained by Europa-UVS can help fill in the gaps in altimetric coverage, significantly improving global shape fits.

Corresponding author: Jacob Abrahams, abrahams@ucsc.edu

Abstract

Europa Clipper will arrive at Jupiter at the end of this decade and will explore Europa through a series of flybys. One of its many goals is to characterize Europa's topography and global shape using the EIS and REASON instruments. In addition, Europa Clipper's UV Spectrograph will observe stars pass behind (be occulted by) Europa. The spectrograph has sufficiently precise timing, corresponding to a topographic precision of order meters, that these occultations can also serve as altimetric measurements. Because of gaps in the REASON radar altimeter coverage imposed by the flyby geometries, the addition of ∼100 occultations results in a substantial improvement in the recovery of Europa's long-wavelength shape. Typically five extra spherical harmonic degrees of topography can be recovered by combining occultations with radar altimetry.

Plain Language Summary

Understanding Europa's topography is crucial to understand the moon for a variety of reasons. One way to quantify the topography is global shape, where we describe the entire surface at once. For example, Earth's rotation causes it to bulge at the equator, and we can describe that bulge with a single number: Earth is on average about 40 km larger at the equator than at the poles. A body's global shape as a whole can be described in a similar way, with a series of amplitudes of prescribed shapes (like an equatorial bulge) referred to as "spherical harmonics". Understanding global shape is important because the ice shell is an inherently global structure, and its history, strength, and behavior often reveal themselves as global features. However, if there are gaps in data coverage, spherical harmonics with features (approximately) smaller than those gaps become unreliable to fit, limiting the resolution of shape models. In this paper, we show that measurements by Europa-UVS of stars passing behind Europa can help to fill gaps in Europa Clipper's topographic coverage and significantly improve our ability to determine Europa's global shape.

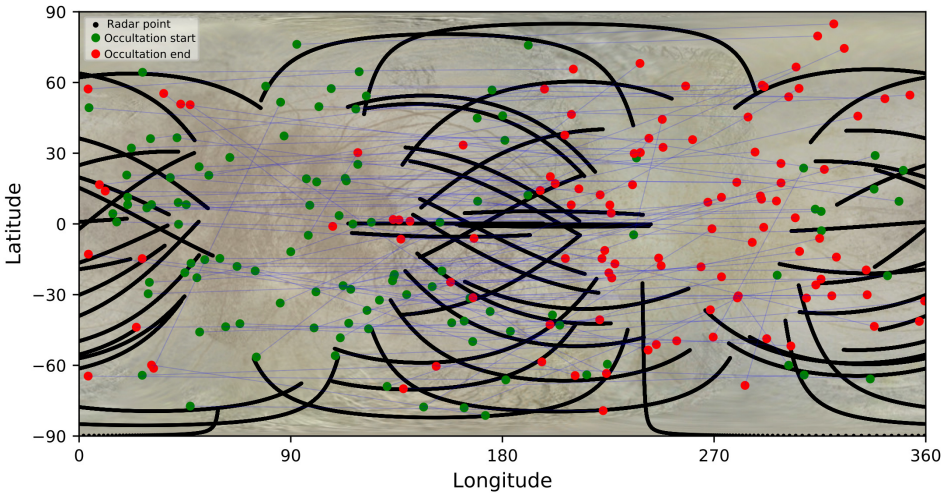

Figure 1. Map of radar altimetry profiles at altitudes <500 km (densely spaced black dots) and likely occultation opportunities (green for ingress and red for egress, individual chords connected by a blue line) for trajectory 19F22. Notably, the radar measurements are concentrated around the subjovian and antijovian points. This results in global shape fits with large misfits at wavelengths smaller than the size of the gaps. The occultation measurements are able to fill in some of these gaps, significantly improving global coverage. Note that this map is based on proposed trajectories that are still evolving, but the general trend of altimetry profiles being concentrated at the sub- and anti-jovian points and occultations being more uniformly distributed comes from inherent orbital constraints. There are 109 total occultations and 283571 radar measurements across 46 separate tracks. Background map created by Björn Jónsson.

1 Introduction

Europa's global shape is only poorly constrained, with our best models inferred from four Galileo limb profiles (Nimmo et al., 2007). Obtaining more precise global and regional topography is important if we want to understand Europa's internal structure and the state of its ice shell (D. Hemingway et al., 2013; Ojakangas & Stevenson, 1989), and is an objective of the Europa Clipper mission (Pappalardo et al., 2019). The primary instruments for determining Europa's global shape are the radar instrument REASON (Radar for Europa Assessment and Sounding: Ocean to Near-surface) (Blankenship et al., 2018) and the visible imager EIS (Europa Imaging System) (Turtle et al., 2019). The main limitation in fitting global shape is the fact that neither the radar tracks (black dots

in Figure 1) nor the EIS limb profiles have complete global coverage, instead having gaps around the poles and longitudes near 90° and 270° as a consequence of Europa Clipper's resonant flyby geometry. Filling in those gaps has the potential to dramatically improve our ability to fit the global shape and its time variation. A similar problem was encountered by the MESSENGER mission to Mercury, and a similar solution was employed: sparse radio occultation measurements of southern hemisphere topography were used to augment dense altimetric measurements of the northern hemisphere (Perry et al., 2015).

In this paper we focus on combining occultations with REASON altimetry to demonstrate the utility of stellar occultations for filling in data gaps and improving our knowledge of Europa's shape. In reality, EIS limb profiles will also contribute, despite suffering from similar gaps to REASON; to keep our analysis simple, and to explore the important role of the radar altimetric cutoff, we do not consider their contributions further below.

Europa Clipper's UV Spectrograph (UVS) (Retherford et al., 2015) will observe stars as they pass behind Europa, with the primary goals of studying potential plumes and a tenuous atmosphere. Notably, however, the instrument's maximum temporal resolution is ∼1 millisecond. Because the apparent velocity of stars relative to Europa is of order 1 km/s, the timing of an occultation is equivalent to a measurement, with an uncertainty on the order of meters, of the relative positions (in the direction of travel) of Europa, Europa Clipper, and the star. If the spacecraft and star positions are well known, this is equivalent to a ∼1 m resolution measurement of the position of Europa's surface. Alternatively, if the star's disappearance and reappearance are both observed, then the spacecraft and star position uncertainty mostly cancel out and the duration of the occultation is equivalent to a ∼1 m resolution measurement of a chord across Europa. In this paper we focus on two-sided occultations, chords, which allow us to ignore uncertainties in spacecraft tracking and stellar catalogues. In reality, many occultations will likely be one-sided; in this case, the analysis would proceed in a similar fashion to that described below, but the effect of these extra uncertainties would need to be considered.

Stellar occultations have the significant benefit of being well distributed across the satellite, meaning they fill in a lot of the radar profiles' gaps, as shown in Figure 1. Although the actual spacecraft tour will differ from those used in this figure, the spatial distribution of the two data sets will remain qualitatively the same. As mentioned above,

in this paper we only consider chords, where we know the time of the star's disappearance and reappearance.

Ice shell structure, and therefore global shape, is a high priority target for Europa Clipper because it is key to understanding several fundamental features of a planetary body. For example, Ojakangas and Stevenson (1989) predicted long-wavelength variations in ice shell thickness (and thus topography) on Europa, caused by spatial variation in tidal heating. This was then investigated by Nimmo et al. (2007) who were able to place upper limits on the amplitude of shell thickness variations using Galileo data. Measurements by Europa Clipper will further refine those constraints, and may be able to detect any nonzero shell thickness variations. A positive detection of the predicted long-wavelength variations would help constrain Europa's shell thickness and rate of heating. If no such variations are detected, then either the shell must be very thin or the base of the shell must have such a low viscosity that it can erase variations as they form.

Measurements of a body's long wavelength shape, typically expressed in terms of spherical harmonic coefficients of degree l and order m, are useful for at least two additional reasons. First, the topographic roughness spectrum of a body may itself contain information about geophysical parameters of interest, such as elastic thickness (Araki et al., 2009; Nimmo et al., 2011), interior rheology (Fu et al., 2017), and surface structure (Ermakov et al., 2019). Second, the ratio of a body's gravity to topography at different values of l - the admittance - captures key information about its structure, and has been employed very successfully around the solar system. For example, admittance has been used to infer the rigidity and weathering of Titan's ice shell (D. Hemingway et al., 2013), the thicknesses and densities of the crusts of Mercury (Sori, 2018) and Enceladus (Iess et al., 2014; D. J. Hemingway & Mittal, 2019), and the compensation state and subsurface rheology on Ceres (Ermakov et al., 2017; Ruesch et al., 2019).

Finally, measuring Europa's diurnal tidal deformation would be helpful in understanding ice shell thickness and rheology (Moore & Schubert, 2000; Wahr et al., 2006; Steinbrügge et al., 2018), and the high precision of occultations suggests they could be helpful in identifying tides. Surface deformation is particularly valuable to measure because it yields one Love number, h_2. When h_2 is combined with a second Love number, k_2 (derived from gravity moments), it becomes possible to obtain a substantially better estimate of the shell thickness than is possible with either measurement alone. Wahr

et al. (2006) lay out this process in detail for Europa. REASON will seek to constrain Europa's tides by looking for time-dependence at the points where radar tracks intersect (Steinbrügge et al., 2018). It would be very valuable if UVS occultations can also help constrain Europa's tides, so we conducted a preliminary search for tides, but as discussed later we find that our expected ∼hundreds of stellar occultations are not sufficient alone to fit tides.

The primary challenge for studying Europa's global shape with radar altimetry is the fact that Europa Clipper will orbit Jupiter and only study Europa during flybys. This means that the measurements it is able to make are limited by orbital dynamics . In particular, Europa Clipper's closest approaches are clustered around Europa's subjovian and antijovian points, resulting in coverage gaps at the centers of the leading and trailing hemispheres, and towards the poles (Figure 1). As we describe later in this paper, gaps of this nature greatly restrict our ability to determine spherical harmonic coefficients. A good rule of thumb is that a gap of X degrees results in a maximum possible recovered degree of $l_{max} \approx 360°/X$. The great advantage of occultation profiles is that they fill in these gaps and thus allow topography to be recovered to higher degrees. The number of available UVS occultation events increases with proximity to Europa, but in principle the occultation measurement works equally well at infinite distance, enabling much more uniform global coverage.

In this paper we explore how combining UV Spectrograph occultations with radar altimetry can improve global shape fits. We demonstrate that adding occultations increases the maximum degree that can be fit and decreases the typical misfit in general.

2 Methods

To explore whether occultation data can help characterize Europa we 1) take an assumed shape model (Section 3.1.4), 2) generate synthetic radar and occultation data from it, and then 3) explore our ability to retrieve our original shape model using those synthetic data. In order to identify what is important for shape fitting, we fit a shape model in three different ways: using only radar data, only occultation data, and both datasets combined (Figure 2). In addition, we explore adding tides to our data (Section 3.2), and what happens when we modify our shape model, our measurement locations, and our measurement precision (Section 3.1). We assume that when they are usable (Sec-

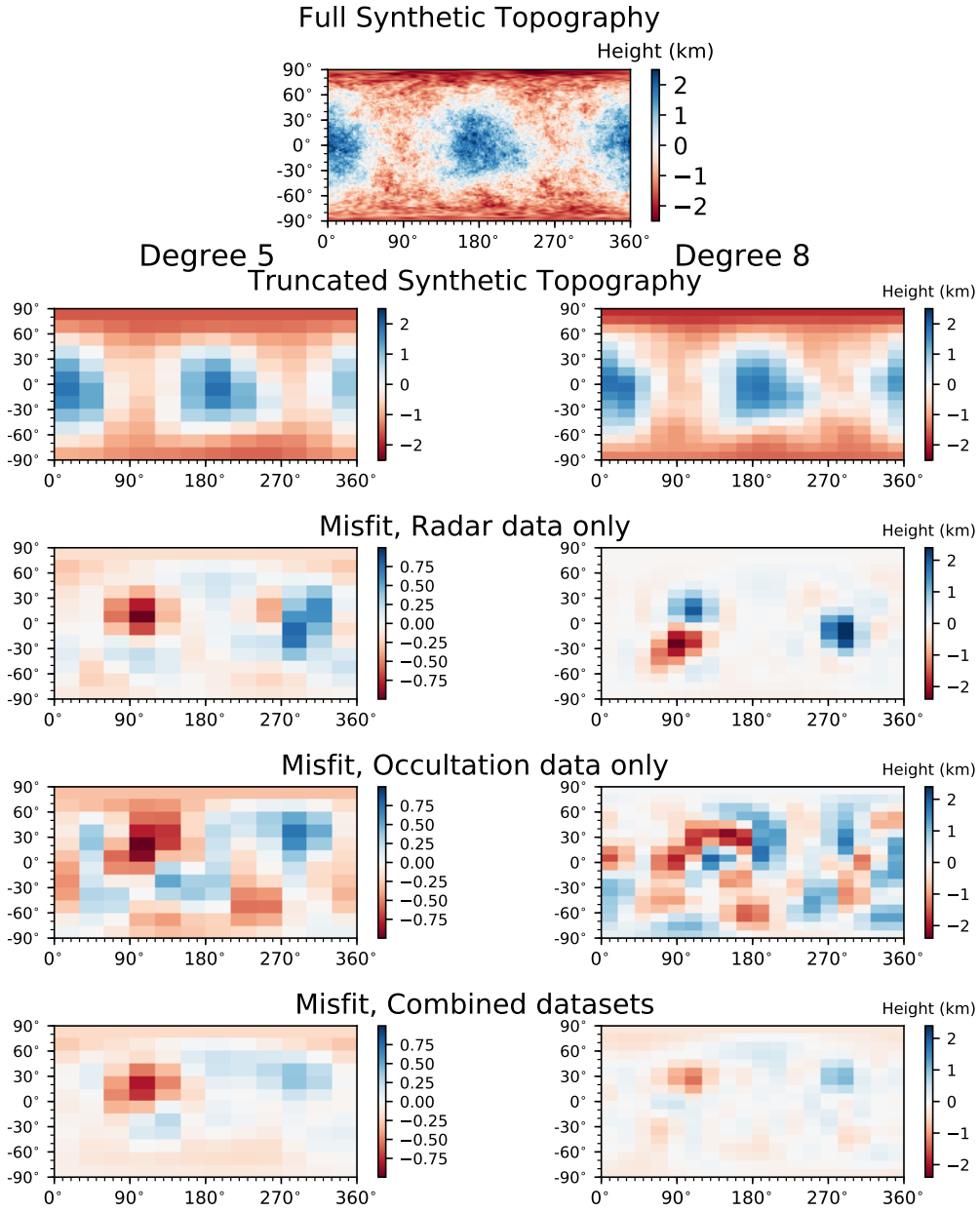

Figure 2. Illustration of fits at two different degrees. The top panel shows the map with which we generate our synthetic data. The first row shows that same map, but truncated at spherical harmonic degrees 5 and 8. Then the next three rows are misfit maps for fits using only radar data, only UVS chords, and with both datasets simultaneously. For each of those fits, we prescribe a degree out to which we want to fit (5 or 8 for this plot) and then attempt to fit all degrees and orders up to that degree. Note that the left and right column misfit maps have different color scales and the degree 8 fits all have ∼2-3 times larger errors than their degree 5 counterparts.

tion 3.1.3) radar data are perfectly precise, and we generally make the same assumption for occultation chords – see Section 3.1.2 for discussion and testing of these assumptions.

We use least-squares to find the set of spherical harmonics that best fit our synthetic data, in a similar fashion to Nimmo et al. (2011). Generically, this involves solving the matrix equation

$$\hat{\boldsymbol{x}} = \left(\underline{\boldsymbol{A}}^T \cdot \underline{\boldsymbol{A}}\right)^{-1} \cdot \underline{\boldsymbol{A}}^T \cdot \boldsymbol{z} \tag{1}$$

where $\hat{\boldsymbol{x}}$ is the vector of coefficients that we want to fit and $\boldsymbol{z}$ is a vector of measurements. For our work, $\hat{\boldsymbol{x}} = \{C_{00}, C_{10}, C_{11}, S_{11}, \cdots, C_{NN}, S_{NN}\}$, the spherical harmonics we want to fit, and $\boldsymbol{z} = \{c_1, c_2, c_3, \cdots, c_M\}$, the set of measured occultation chord lengths. The elements of the matrix $\underline{\boldsymbol{A}}$ are defined by $A_{ij} = \frac{\partial z_i}{\partial x_j}$. Further details for computing $\underline{\boldsymbol{A}}$ and our spherical harmonic conventions are in Appendix A. Each term in the matrix $\underline{\boldsymbol{A}}$ can be well approximated analytically, and we solve Equation 1 numerically.

If the topographic power spectrum is known a priori, an additional damping term can be added to Equation 1 to avoid large oscillations in areas with no data coverage (Nimmo et al., 2011). We did not apply such a term here because we are interested in how well we can recover topography without imposing additional assumptions.

We can also, optionally, include an extra term in $\hat{\boldsymbol{x}}$ corresponding to tidal amplitude, and attempt to fit Europa's time-varying shape as it deforms over its orbit, as discussed further in Section 3.2.

Because we do not yet know Europa's real shape precisely enough, this paper fits synthetic data intended to approximate what Europa Clipper will encounter. We assume Europa's shape, calculate what the radar and occultation measurements would be for that assumed shape, and then run our fitting script on those synthetic measurements. The primary shape we assume is designed to match the power spectrum in the global fits in Nimmo et al. (2007). Our nominal shape model is discussed more in Section 3.1.4 and is shown in the first panel of Figure 2.

3 Results

Figure 2 illustrates our nominal shape model, as well as that shape model truncated at two different spherical harmonic degrees and our attempts to fit those truncated shape models. Broadly, we are able to fit low degrees and our fits degrade at higher degrees.

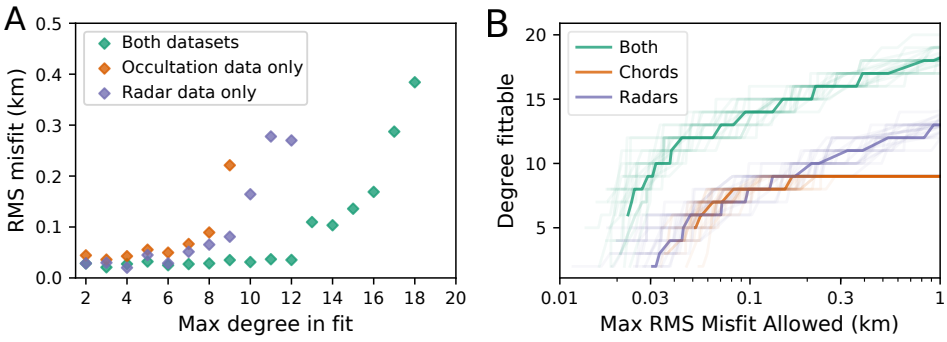

Figure 3. A) Average misfit as a function of the total degree we attempt to fit for our nominal shape model. Combining UVS chords with radar data marginally improves fits in general, and significantly extends the total degree that can be well fit. In panel B) we assume there is some cutoff misfit considered "acceptable", and as a function of that cutoff we show the maximum spherical harmonic degree that the individual and combined datasets are able to achieve. We run a suite of fits, varying our shape models according to Section 3.1.4, and plot each individual run as a faint line. The ensemble average is plotted with the solid lines.

As expected, the errors in the radar-derived shape model are largest around the leading and trailing hemispheres, where there are no observations. Combining radar with occultation data decreases the misfit in general, because we are using more data. More importantly though, it increases the maximum spherical harmonic degree that can be fit at all because the occultation chords fill in the radar altimetry gaps.

Figure 3 shows that combining occultation data with radar data allows significantly better fits than either dataset alone. In particular, Figure 3a shows the radar-derived topography breaks down above $l = 9$, which is consistent with the existence of gaps approximately 45° wide in the radar coverage (Figure 1). The addition of occultation points filling in these gaps allows the topography to be recovered up to $l = 12$. Similarly, Figure 3b shows a consistent improvement of roughly 5 extra spherical harmonic degrees when occultations are added to the radar data. Finally, Table 1 lists the uncertainties in some recovered low-order spherical harmonics, again showing the improvement obtained by adding in the occultation points.

	C_{20}	C_{22}	C_{40}	C_{44}
Actual (m)	-581	594	-43	42
Radar only uncertainty (m)	35	36	42	30
Chord only uncertainty (m)	45	87	25	53
Combined uncertainty (m)	18	26	22	21

Table 1. Precision for our fits for important spherical harmonic coefficients. "Actual" refers to the injected spherical harmonic amplitude. Uncertainties are determined by finding the RMS misfit for individual coefficients over a suite of model runs in which we randomly perturb the input shape model and then fit up to degree and order 5.

3.1 Sensitivity to Inputs

3.1.1 Number of Occultations

The number of stellar occultations that UVS can observe is highly dependent on tour geometry and data downlink allocation, so it is likely that we receive a different number (possibly a very different number) of occultations than the 109 in our assumed mission plan (trajectory "19F22"). We find that in general, fit quality scales approximately with the square root of the number of occultations. For fits using only chords, the maximum degree that can be fit also scales with the square root of the number of chords, but that effect is more minor for combined (occultation and radar) fits. Overall, more chords unsurprisingly makes for better fits, but while many tours have roughly 200 (rather than the baseline 100) occultation opportunities, it is unlikely that we will collect enough chords to dramatically change the conclusions of this paper.

3.1.2 Precision of Measurements

For the bulk of this work, we assumed that measurements were perfectly precise. The motivation for this assumption is that for global fits, we expect our misfit to arise primarily from gaps in global coverage, rather than poor data quality where we have data. That said, it is of course true that at some point, measurement uncertainty will become

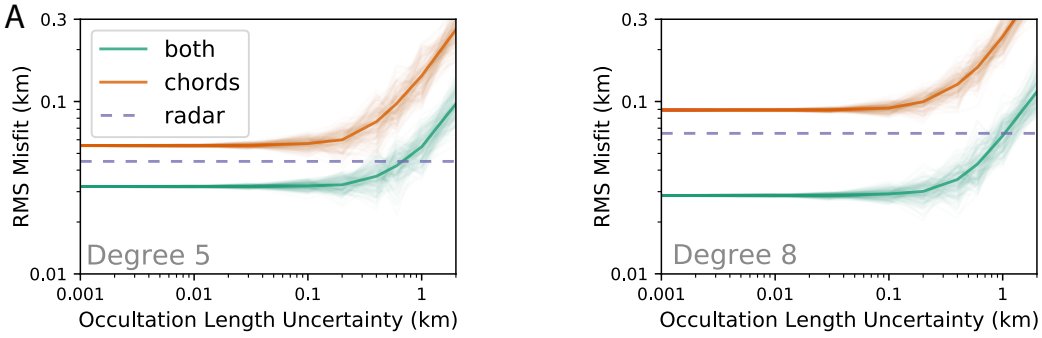

Figure 4. The effect of measurement precision on retrievals. We inject random noise into the length of each occultation, and then observe the misfit. Panel **a** is trying to fit shape up to degree/order 5, and panel **b** is trying to fit shape up to degree/order 8. Each faint line is an individual set of chords with varying amounts of noise added, and the dark lines are the ensemble average. We do not inject noise into the radar data; perfectly precise radar retrievals are indicated by the dotted lines for comparison.

important. To determine the level where measurement precision becomes the dominant source of error, we inject noise into our data.

Figure 4 shows the impact of varying the UVS measurement precision. Notably, fit quality only really begins to degrade when the uncertainty reaches 300 m, and shifts significantly with an uncertainty of about 1 km. The main source of uncertainty in the length of a chord is how precisely timed the stellar ingress and egress are. UVS can collect data at a cadence of up to 1 ms in its pixel-list mode or up to 10 ms in its histogram mode (Retherford et al., 2015). If the spacecraft is moving at 10 km/s relative to Europa, even the 10 ms cadence is only an uncertainty of 100 m. If, instead of collecting chords, observations are only made on one side of an occultation, then the spacecraft position, spacecraft pointing, and stellar position can be significant sources of error, and uncertainties in those quantities would need to be under $\sim$1 km for UVS occultations to be useful topographic constraints. Overall, occultation timing precision is not expected to degrade global shape fits for two-sided occultations. For one-sided occultations further analysis would be needed, because of the potential role of spacecraft and satellite position uncertainties.

3.1.3 Altitude Cutoff for Radar

One of the biggest uncertainties in this work is the range to which useful radar altimetric returns will be obtained, and thus the total length of each altimetry profile. Over the course of a single flyby, Europa Clipper's distance from Europa varies significantly. It is not yet clear within what distance REASON will be able to get a reliable surface return from Europa, because that altitude cutoff depends on the characteristics of Europa's surface, but the baseline for the instrument is 1000 km (pink in figure 5). Steinbrügge et al. (2018) discuss REASON's performance in detail, but, broadly, the effective altimetric range is determined by a combination of the signal-to-noise ratio of the instrument, and the fact that when using the radar instrument as an altimeter, the "surface" that the radar detects is not necessarily the sub-spacecraft point. Instead, it is the nearest region on Europa's surface which is locally flat and oriented properly with respect to the spacecraft. For example, a mountain near (but not on) the spacecraft trajectory can plausibly be closer to the spacecraft than the surface directly below the spacecraft, and depending on the orientation of its flanks it may produce a misleading return. Further uncertainties arise from the ionosphere of Europa which delays the radio signal (Grima et al., 2015) leading to systematic errors unless corrected by using both frequencies available to the REASON instrument (Scanlan et al., 2019). As a result, the exact performance of radar altimetry depends on uncertain characteristics of Europa and cannot be fully known until arrival. We incorporate these limitations, in a simplified form, by assuming that there is some distance inside of which REASON becomes a reliable altimeter.

For the nominal plots in this work, we assume an altitude cutoff of 500 km. This is an arbitrary choice, and different from REASON's baseline of 1000 km. We chose 500 km primarily because that is the altitude where radar altimetry and occultation chords have roughly the same performance for fitting global shape, allowing the improvements from combining datasets to be most easily seen. Figure 5 illustrates what happens when we vary this assumption. In general, the higher the radar altitude cutoff, the better the fits. However, although radar data alone perform better when they extend to higher altitudes, we observe that adding the occultation chords always helps. Thus, although it is hard to accurately predict Europa Clipper's ability to fit global shape using radar alone, it is clear that regardless of the radar performance, occultation chords should always improve those fits.

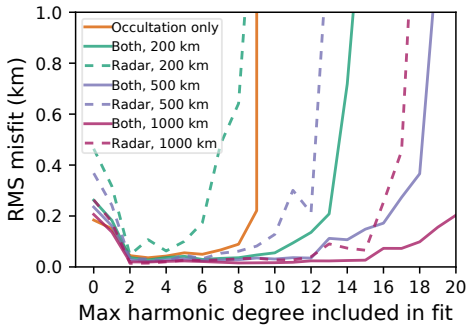

Figure 5. Varying the altitude at which the radar data are cut off, showing the evolution of misfit as a function of the degree included in the fit for radar data collected below 200 km, 500 km, and 1000 km. The 1000 km data have roughly twice as many total data points, and the 200 km data have roughly half as many. Radar alone fits the shape better if higher altitude data are included, but regardless of the cutoff, UVS chords always improve the radar fits. One noteworthy feature is the fact that the fits at degrees 0 and 1 are quite bad, and they improve significantly at degree 2, demonstrating the significance of Europa's permanent tidal bulge.

3.1.4 Shape Model Used

To explore the value of occultation chords, we need simulated data to fit, which requires a shape model to generate those data. Without a good current model of Europa's global shape, we needed to assume one. Our nominal topographic model consists of three components. The first is the degree-two shape arising from tidal and rotational distortion alone. The second is topography arising from shell thickness variations due to tidal heating, resulting in power at both l=2 and l=4. These two components are the same as the nominal model in Table 3 of Nimmo et al. (2007). The final component consists of randomly-generated topography up to l=180 ($\approx$ 50 km wavelength) and assuming a power-law slope of -1, based on Europa limb profiles (Nimmo et al., 2011). Our model does not include short-wavelength roughness because, as shown in Figure 4, topography with an amplitude less than about 100 m does not impact our fit quality.

One potential problem with occultations, as with limb profiles, is that they record the highest point in the line of sight, which may not be at the expected location (on the limb) (Perry et al., 2015, e.g.). A synthetic analysis by Nimmo et al. (2010) showed that for the icy satellite Rhea this effect did not bias the recovery of long-wavelength topog-

raphy appreciably. Since Europa is much smoother than Rhea, we expect the same result to hold here.

To ensure we are not just fitting pathologies in one particular model, we test a few different modifications. First, we take our nominal power spectrum, and randomly generate spherical harmonic coefficients that match it, and run our model on a suite of these randomly generated Europas. In addition, we take those power spectra and increase or decrease their amplitudes (preserving their slopes) beyond degree 3, in order to explore whether more or less topography impacts our fits. Finally, we ran our model on a global map of Earth's Moon, rescaled to match Europa's radius and tidal bulge. Our results across all of these modifications were broadly similar, so we consider our results robust to variations in the specific shape model chosen.

3.2 Diurnal Tide Fits

Europa Clipper's ability to fit Europa's diurnal tides, and the potential for stellar occultations to improve those fits, is a very important question but requires detailed radar models that lie outside the scope of this paper. We restrict our analysis to whether occultation data alone can detect tides, and find the answer is most likely no. To do this, we inject a time varying signal into the degree 2 harmonics in our shape model and propagate it into our synthetic data, and we modify the vector we are trying to fit ($\hat{\boldsymbol{x}}$ in Section 2) so that in addition to a set of spherical harmonics, it contains a parameter for the tidal amplitude. Then we can compare our best fit tidal amplitude to our injected tidal amplitude and assign a misfit. Figure 6 shows the distribution of those misfits. Europa's diurnal tidal deformation is expected to have an amplitude of 30 m (Moore & Schubert, 2000), and our tidal retrieval misfits are normally distributed with a standard deviation of roughly 60 m, so we cannot reliably detect tidal deformation and we certainly cannot precisely constrain its amplitude. The main reason for this is that no two occultations are likely to occur at the same location (unlike radar data, which can specifically look at the intersections of radar tracks), so there is a degeneracy between local topography and global deformation. We find our tidal misfit decreases with the square root of the number of occultations and with the square root of the amplitude of Europa's topographic power spectrum. Thus, if we get many more chords than we expect, or if Europa has much less topography than expected, occultations have the potential to detect tides (though this would probably take on the order of 1000 occultations, and a mean-

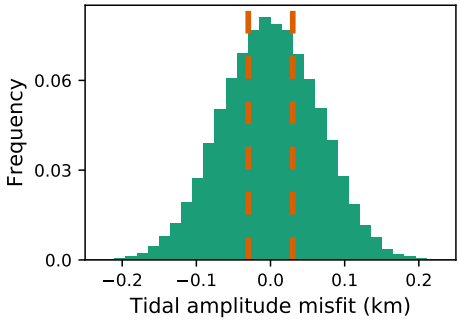

Figure 6. Injecting diurnal tidal deformation into the synthetic occultation data, and trying to retrieve its amplitude. Histogram shows the misfit in tidal retrievals, and the red dotted lines show the expected real amplitude of Europa's tides. This distribution is independent of the injected tidal amplitude across a range of amplitudes from one meter to tens of kilometers. These results indicate that UVS occultations alone are not sufficient to reliably detect Europa's tides. Note that "frequency" refers to the fraction of the trials in each bin, it does not integrate to 1.

ingful constraint on their amplitude would take significantly more). Occultations alone probably cannot significantly constrain Europa's tidal deformation.

Ultimately, the important question is not whether occultation data can constrain tides, but whether all of Europa Clipper's altimetry can combine to constrain tides. However, unlike previous topics in this paper, our simple model of the radar data as perfectly precise measurements is inadequate. For the bulk of this work, we have taken the conservative assumption of perfectly accurate radar data and demonstrated that, even in this case, occultation chords can still improve the global shape recovery. However, detecting diurnal tidal deformation with perfect radar data is not difficult – the reason tides are likely to be difficult to detect is that the uncertainty in the radar altimetry is significantly more complicated than just instrument noise (Steinbrügge et al., 2018). This means that testing whether occultation data can help radar data to detect tidal deformation requires a much more complete radar model that captures the *limitations* of the radar data, as well as a recreation of the treatment of "cross-over" data that the REASON teams plans. We recommend that future work explore whether occultation and radar data combined allow higher quality tide retrievals, but do not pursue that goal here.

4 Discussion and Conclusions

The goal of this work is to highlight the value of stellar occultations for global shape fits, in order to inform future trajectory selection, data volume prioritization, and ultimately to help improve the quality of Europa Clipper mission products. Because these are measurements that were already planned for other purposes, this work shows that we can improve Clipper's ability to constrain Europa's ice shell without any modifications to the mission architecture. The primary value of occultations is the fact that they are fairly uniformly distributed across Europa. This means they have little value for studying local topography, but are perfectly suited for constraining Europa's long-wavelength global shape.

An additional tool to constrain Europa's shape, which has not been included in this analysis, is the Europa Imaging System (EIS) instrument (Turtle et al., 2019) which will image, among other things, the limb of Europa in order to produce topographic profiles. These limb profiles have the advantage of being linear profiles, rather than point measurements like occultations, and suffer somewhat less from gaps than do the radar profiles. However, the precision of each limb measurement, conservatively 0.2 pixels, is worse by more than an order of magnitude compared to the occultation precision. In any event, limb profiles have the potential to provide further geographically disjoint data, and further improvements to the long-wavelength shape of Europa.

We find that stellar occultations from UVS are very valuable for fitting Europa's global shape. Future work can further refine our understanding of the value of these chords and how best to use them to understand topography. For a very wide range of radar performances, stellar occultations improve the quality of long-wavelength fits, provide an independent check on data collected by other instruments, and improve the spatial resolution that global fits will be able to achieve.

Acknowledgments

We thank Luciano Iess for early conversations related to the utility of astrometric observations planned for JUICE-UVS, Zibi Turtle for valuable feedback, and Björn Jónsson for the background map in Figure 1. We also thank the creators of Pyshtools for their incredibly valuable python package. The code and synthetic data used in this paper are

available in the Dryad repository at `https://doi.org/10.7291/D1K968`. Parts of this work were supported by the REASON subcontract to UCSC UTA16-000107.

References

Araki, H., Tazawa, S., Noda, H., Ishihara, Y., Goossens, S., Sasaki, S., ... Shum, C. (2009). Lunar global shape and polar topography derived from Kaguya-LALT laser altimetry. *Science*, *323*(5916), 897–900. doi: 10.1126/science.1164146

Blankenship, D., Ray, T., Plaut, J., Moussessian, A., Patterson, W., Romero-Wolf, A., ... Team, R. S. (2018, jul). REASON for Europa. In *42nd cospar scientific assembly* (Vol. 42, pp. B5.3–55–18). Retrieved from `https://ui.adsabs.harvard.edu/abs/2018cosp...42E.377B`

Ermakov, A. I., Fu, R. R., Castillo-Rogez, J. C., Raymond, C. A., Park, R. S., Preusker, F., ... Zuber, M. T. (2017). Constraints on Ceres' Internal Structure and Evolution From Its Shape and Gravity Measured by the Dawn Spacecraft. *Journal of Geophysical Research: Planets*, *122*(11), 2267–2293. doi: 10.1002/2017JE005302

Ermakov, A. I., Kreslavsky, M. A., Scully, J. E., Hughson, K. H., & Park, R. S. (2019). Surface Roughness and Gravitational Slope Distributions of Vesta and Ceres. *Journal of Geophysical Research: Planets*, *124*(1), 14–30. doi: 10.1029/2018JE005813

Fu, R. R., Ermakov, A. I., Marchi, S., Castillo-Rogez, J. C., Raymond, C. A., Hager, B. H., ... Russell, C. T. (2017). The interior structure of Ceres as revealed by surface topography. *Earth and Planetary Science Letters*, *476*, 153–164. Retrieved from `http://dx.doi.org/10.1016/j.epsl.2017.07.053` doi: 10.1016/j.epsl.2017.07.053

Grima, C., Blankenship, D. D., & Schroeder, D. M. (2015). Radar signal propagation through the ionosphere of Europa. *Planetary and Space Science*, *117*, 421–428. Retrieved from `http://dx.doi.org/10.1016/j.pss.2015.08.017` doi: 10.1016/j.pss.2015.08.017

Hemingway, D., Nimmo, F., Zebker, H., & Iess, L. (2013). A rigid and weathered ice shell on Titan. *Nature*, *500*(7464), 550–552. Retrieved from `http://dx.doi.org/10.1038/nature12400` doi: 10.1038/nature12400

Hemingway, D. J., & Mittal, T. (2019). Enceladus's ice shell structure as a window

on internal heat production. *Icarus*, *332*, 111–131. Retrieved from `https://doi.org/10.1016/j.icarus.2019.03.011` doi: 10.1016/j.icarus.2019.03.011

Iess, L., Stevenson, D. J., Parisi, M., Hemingway, D. J., Jacobson, R. A., Lunine, J. I., ... Tortora, P. (2014). The Gravity Field and Interior Structure of Enceladus. *Science*, *344*, 78–81. doi: 10.1126/science.1250551

Moore, W. B., & Schubert, G. (2000). The Tidal Response of Europa. *Icarus*, *147*(1), 317–319. doi: 10.1006/icar.2000.6460

Nimmo, F., Bills, B. G., & Thomas, P. C. (2011). Geophysical implications of the long-wavelength topography of the Saturnian satellites. *Journal of Geophysical Research E: Planets*, *116*(11), 1–12. doi: 10.1029/2011JE003835

Nimmo, F., Bills, B. G., Thomas, P. C., & Asmar, S. W. (2010). Geophysical implications of the long-wavelength topography of Rhea. *Journal of Geophysical Research E: Planets*, *115*(10), 1–12. doi: 10.1029/2010JE003604

Nimmo, F., Thomas, P. C., Pappalardo, R. T., & Moore, W. B. (2007). The global shape of Europa: Constraints on lateral shell thickness variations. *Icarus*, *191*(1), 183–192. doi: 10.1016/j.icarus.2007.04.021

Ojakangas, G. W., & Stevenson, D. J. (1989). Polar wander of an ice shell on Europa. *Icarus*, *81*(2), 242–270. doi: 10.1016/0019-1035(89)90053-5

Pappalardo, R. T., Senske, D., Korth, H., Becker, T. M., Blaney, D. L., Blankenship, D. D., ... Westlake, J. H. (2019). The Europa Clipper: Science and Mission. In *Agu fall meeting* (pp. P53B–06).

Perry, M. E., Neumann, G. A., Phillips, R. J., Barnouin, O. S., Ernst, C. M., Kahan, D. S., ... Oberst, J. (2015). The low-degree shape of Mercury. *Geophysical Research Letters*, *42*(17), 6951–6958. doi: 10.1002/2015GL065101

Retherford, K. D., Gladstone, G. R., Greathouse, T. K., Steffl, A., Davis, M. W., Feldman, P. D., ... Walther, B. C. (2015). The Ultraviolet Spectrograph on the Europa Mission (Europa-UVS). In *Agu fall meeting* (pp. P13E–02).

Ruesch, O., Genova, A., Neumann, W., Quick, L. C., Castillo-Rogez, J. C., Raymond, C. A., ... Zuber, M. T. (2019). Slurry extrusion on Ceres from a convective mud-bearing mantle. *Nature Geoscience*, *12*(July). Retrieved from `http://www.nature.com/articles/s41561-019-0378-7` doi: 10.1038/s41561-019-0378-7

Scanlan, K. M., Grima, C., Steinbrügge, G., Kempf, S. D., Young, D. A., &

Blankenship, D. D. (2019). Geometric determination of ionospheric total electron content from dual frequency radar sounding measurements. *Planetary and Space Science*, *178*(June), 104696. Retrieved from https://doi.org/10.1016/j.pss.2019.07.010 doi: 10.1016/j.pss.2019.07.010

Sori, M. M. (2018). A thin, dense crust for Mercury. *Earth and Planetary Science Letters*, *489*, 92–99. Retrieved from https://doi.org/10.1016/j.epsl.2018.02.033 doi: 10.1016/j.epsl.2018.02.033

Steinbrügge, G., Schroeder, D. M., Haynes, M. S., Hussmann, H., Grima, C., & Blankenship, D. D. (2018). Assessing the potential for measuring Europa's tidal Love number h2 using radar sounder and topographic imager data. *Earth and Planetary Science Letters*, *482*(2018), 334–341. Retrieved from https://doi.org/10.1016/j.epsl.2017.11.028 doi: 10.1016/j.epsl.2017.11.028

Turtle, E. P., McEwen, A. S., Collins, G. C., Daubar, I. J., Ernst, C. M., Fletcher, L., ... Bland, M. (2019, mar). The Europa Imaging System (EIS): High-Resolution, 3-D Insight into Europa's Geology, Ice Shell, and Potential for Current Activity. In *Lunar and planetary science conference* (p. 3065).

Wahr, J. M., Zuber, M. T., Smith, D. E., & Lunine, J. I. (2006). Tides on Europa, and the thickness of Europa's icy shell. *Journal of Geophysical Research E: Planets*, *111*(12), 1–10. doi: 10.1029/2006JE002729

Computing $\underline{\boldsymbol{A}}$

To compute A_{ij} we begin with the fact that the topography at any point (θ, ϕ) is given, in spherical harmonics, by

$$h = \sum_{l,m=0}^{\infty} C_{lm} \cos(m\phi) P_{lm}(\cos\theta) + S_{lm} \sin(m\phi) P_{lm}(\cos\theta) \tag{1}$$

For the measurements that are topographic points (i.e. radar altimetry, not chords), computing $\underline{\boldsymbol{A}}$ is straightforward. For example, recalling that $\hat{\boldsymbol{x}} = \{C_{00}, C_{10}, C_{11}, S_{11}, \cdots, C_{NN}, S_{NN}\}$, and for radar data $\boldsymbol{z} = \{h_1, h_2, h_3, \cdots, h_M\}$

$$A_{23} = \frac{\partial z_2}{\partial x_3} \tag{2}$$

$$= \frac{\partial h_2}{\partial C_{11}} \tag{3}$$

$$= \cos(\phi_2) P_{11}(\cos\theta_2) \tag{4}$$

which, crucially, contains no elements of $\hat{\boldsymbol{x}}$, so $\hat{\boldsymbol{x}}$ can be calculated without any assumption a priori. However, chords are more complicated. First we need to get the chord length itself in terms of spherical harmonics. The chord length between two surface points h_{i1} and h_{i2} can be computed by treating them as a triangle with the angle between them as γ. The law of cosines gives us the length, $c = \sqrt{h_{i1}^2 + h_{i2}^2 - 2h_{i1}h_{i2}\cos\gamma_i}$. Trying to compute an element of A reveals our problem

$$A_{ij} = \frac{\partial c_i}{\partial C_{lm}} = \frac{\partial c_i}{\partial h_{i1}} \frac{\partial h_{i1}}{\partial C_{lm}} + \frac{\partial c_i}{\partial h_{i2}} \frac{\partial h_{i2}}{\partial C_{lm}} \tag{5}$$

$$= \frac{h_{i1} - h_{i2}\cos\gamma_i}{c_i} \cos(m\phi_{i1}) P_{lm}(\cos\theta_{i1}) + \frac{h_{i2} - h_{i1}\cos\gamma_i}{c_i} \cos(m\phi_{i2}) P_{lm}(\cos\theta_{i2}) \tag{6}$$

Notably, A_{ij} depends on h_{i1} and h_{i2}. This is a problem, because our measurement is only of c_i. Computing h_{i1} and h_{i2} requires assuming values of C_{lm}, but that is precisely what we are trying to fit. This means that it is impossible to compute elements of $\underline{\boldsymbol{A}}$ which are independent of $\hat{\boldsymbol{x}}$ to allow us to solve for $\hat{\boldsymbol{x}}$. One solution to this is to solve $\hat{\boldsymbol{x}}$ iteratively, beginning with an assumed shape $\hat{\boldsymbol{x}}_0$, using this to compute a new $\hat{\boldsymbol{x}}_1$, and repeating until the result converges. This approach has the advantage of it being clear when a self consistent result is found. Another approach is to note that for a hydrostatic planet (like Europa), topography is a small perturbation on the overall radius and we can reasonably assume to zeroth order that $h_1 \approx h_2 \approx R$, the planet's radius. Then, a bit

of trigonometry tells us that $\frac{h_1 - h_2\cos\gamma}{c} \approx \frac{R(1-\cos\gamma)}{2R\sin\frac{\gamma}{2}} = \sin\frac{\gamma}{2}$, and γ is calculable from $(\theta_1, \phi_1, \theta_2, \phi_2)$. This assumption, that $h_1 \approx h_2 \approx R$, allows us to calculate $\underline{\boldsymbol{A}}$ independently of $\hat{\boldsymbol{x}}$, as

$$A_{ij} = \frac{\partial c_i}{\partial C_{lm}} = \frac{\partial c_i}{\partial h_{i1}}\frac{\partial h_{i1}}{\partial C_{lm}} + \frac{\partial c_i}{\partial h_{i2}}\frac{\partial h_{i2}}{\partial C_{lm}} \tag{7}$$

$$= \sin\frac{\gamma_i}{2}\Big[\cos(m\phi_{i1})P_{lm}(\cos\theta_{i1}) + \cos(m\phi_{i2})P_{lm}(\cos\theta_{i2})\Big] \tag{8}$$

$$= \sqrt{\sin^2\left(\frac{\phi_1-\phi_2}{2}\right) + \cos\phi_1\cos\phi_2\sin^2\left(\frac{\theta_1-\theta_2}{2}\right)}\Big[\cos(m\phi_{i1})P_{lm}(\cos\theta_{i1}) + \cos(m\phi_{i2})P_{lm}(\cos\theta_{i2})\Big] \tag{9}$$

Note that if $\hat{\boldsymbol{x}}_j$ were an S_{lm} instead of C_{lm} the solution would be the same except for the $\cos(m\phi)$ terms would be replaced by $\sin(m\phi)$. To confirm that this approximation works, we calculated it multiple ways: using the approximation in Equation 9, using an iterative solution, and a simple (and extremely slow) gradient descent solution that tries to minimize the misfit by randomly making small adjustments to $\{C_{lm}\}$ until a local minimum misfit is found. All of these solutions give the same result (except when the gradient descent gets trapped in a non-global minimum), so we stick with Equation 9 which is the fastest and cleanest.